The Journal of Experimental Biology 212, 3365-3376
Published by The Company of Biologists 2009
doi:10.1242/jeb.034454

The vortex wake of blackcaps (*Sylvia atricapilla* L.) measured using high-speed digital particle image velocimetry (DPIV)

L. C. Johansson* and A. Hedenström

Department of Theoretical Ecology, Lund University, Ecology Building, SE-223 62 Lund, Sweden

*Author for correspondence (christoffer.johansson@teorekol.lu.se)

Accepted 22 July 2009

SUMMARY

Reconstructing the vortex wake of freely flying birds is challenging, but in the past few years, direct measurements of the wake circulation have become available for a number of species. Streamwise circulation has been measured at different positions along the span of the birds, but no measurements have been performed in the transverse plane. Recent findings from studies of bat wakes have pointed to the importance of transverse plane data for reconstructing the wake topology because important structures may be missed otherwise. We present results of high-speed DPIV measurements in the transverse plane behind freely flying blackcaps. We found novel wake structures previously not shown in birds, including wing root vortices of opposite as well as the same sign as the wing tip vortices. This suggests a more complex wake structure in birds than previously assumed and calls for more detailed studies of the flow over the wings and body, respectively. Based on measurements on birds with and without a tail we also tested hypotheses regarding the function of the tail during steady flight. We were unable to detect any differences in the wake pattern between birds with and without a tail. We conclude that the birds do not use their tail to exploit vortices shed at the wing root during the downstroke. Neither did we find support for the hypothesis that the tail should reduce the drag of the bird. The function of the tail during steady flight thus remains unclear and calls for further investigation in future studies.

Supplementary material available online at http://jeb.biologists.org/cgi/content/full/212/20/3365/DC1

Key words: aerodynamics, birds, DPIV, flight, vortex wake.

INTRODUCTION

Traditionally, the study of bird aerodynamics has been restricted to kinematic analyses and modelling of force generation, simplified to varying degrees (Brown, 1953; Norberg, 1975; Norberg, 1990, Hedrick et al., 2002; Hedrick et al., 2004). But, in the past few years, direct measurements of the wake circulation of free-flying birds have become available for a number of species, allowing a direct estimate of the forces generated (Spedding et al., 2003; Warrick et al., 2005; Hedenström et al., 2006a; Hedenström et al., 2006b; Rosén at al., 2007; Henningsson et al., 2008; Tobalske et al., 2009). Circulation has been measured in the streamwise vertical plane at different positions along the span of the birds, but none of these species have been studied in the transverse plane [with the exception of hovering humming birds (Warrick et al., 2005)]. Recent findings from studies of bat wakes have pointed to the importance of transverse plane data for the reconstruction of the wake topology because important structures may be otherwise missed (Hedenström et al., 2007; Johansson et al., 2008). The suggested vortex wake model for bats (Hedenström et al., 2007) is more complex than the ones suggested for birds (Spedding et al., 2003; Henningsson et al., 2008) and includes streamwise structures (for example vortices shed at the wing root) not suggested by the bird data (Spedding et al., 2003). Whether these differences between birds and bats in the suggested wake models are due to real differences or rather to the lack of appropriate data in the bird's case is thus an open question.

One possible cause for a difference in the wakes between birds and bats studied so far could be that birds have a tail, while the bat species studied lack a tail or have an intendation between the legs ('negative' tail, where the trailing edge of the tail is cranial to the trailing edge of the wings). The tail of birds has been suggested to have at least two functions: providing additional aerodynamic force to improve manoeuvring (Thomas, 1993; Thomas, 1997) or as a modulator of the flow behind the body of the bird (Maybury and Rayner, 2001). The second function relates to the observation by Maybury and Rayner (Maybury and Rayner, 2001), who found a lower drag of mounted starling bodies with a tail when compared with bodies without a tail. They suggested that the tail functions as a 'splitter plate', reducing the width of the wake and therefore also the drag (Maybury and Rayner, 2001). Here we mainly focus on a different hypothesis for modulating the flow behind a bird; namely, that the function of the tail is to interact with wing root vortices, shed as a result of spanwise circulation gradients of flapping wings, and thereby reducing the cost of flight by extracting some of the energy shed into the wake by the wings. This hypothesis originates from the findings that bat wakes consist of vortices, of opposite sign to the wing tip vortices, near the wing root of two tailless bat species (Hedenström et al., 2007; Johansson et al., 2008; Hedenström et al., 2009). Even though no studies of the wake in the transverse plane have been performed for forward flight in birds (where these vortices would be visible), the available data have not indicated any existence of wing root vortices in birds (Spedding et al., 2003; Hedenström et al., 2006a; Hedenström et al., 2006b; Rosén et al., 2007). In bats there is a gradient in the circulation along the span, with decreasing values towards the body, a characteristic associated with the shedding of streamwise vortices (Rossow, 1973). In birds, no such gradient has been found, except in swifts *Apus apus* where

a reduced circulation behind the body relative to the wings occurs (Henningsson et al., 2008). Hence, a potential function of the tail could be to utilize the induced flow generated by these wing root vortices, to increase the lift production of the whole animal and thereby reduce the cost of generating lift. This could also unify the vortex structure of the two wings, resulting in the suggested wake models for birds (Spedding et al., 2003; Henningsson et al., 2008).

Here we used a high-speed digital particle image velocimetry (DPIV) system (Hedenström et al., 2009) to measure the wake in the transverse plane of blackcaps, *Sylvia atricapilla*, a migratory passerine species not previously studied using DPIV. This allowed us to reconstruct a three-dimensional model of the bird wake based on multiple measurements from each wing beat. Using the inferred wake model we tested whether the wake of blackcaps differs from bat wake models and from previously suggested bird wake models. Furthermore, we addressed the question of the tail's function by comparing the wakes, qualitatively and quantitatively, of one blackcap with and one without a tail over a range of flight speeds.

MATERIALS AND METHODS

Experimental animals

The experiments were approved by the Lund University ethical board (M153-05). We used two blackcap individuals. One of the individuals had shed all of its tail feathers prior to the experiments. This accidental fright-moulting event allowed us to study the effect of the tail on the vortex wake of these birds during steady level flight. Between experiments, the birds were kept in cages with access to mealworms and vitamin-enriched water. Wing span and wing area were measured from images with the wings spread as prescribed by Pennycuick (Pennycuick, 1989), using a custom-written program in Matlab (MathWorks, Natick, MA, USA). Body mass was measured using an electronic balance after each experimental session. The relevant morphological parameters of the two individuals are summarized in Table 1.

The training procedure was as follows. The bird was first introduced to the wind tunnel whilst perched on a hand-held stick. A net sealed off the test section both upstream and downstream. On the second day the wind tunnel was turned on at a speed close to the calculated minimum power speed U_{mp} and the perch was lowered, at which point the bird started to fly spontaneously. Whenever the bird tried to land anywhere but on the perch, the perch was brought to the bird, making it climb onto the perch. This procedure was repeated for as long as it took to get the bird to comfortably perch on the stick and nowhere else. At that point the hand-held perch was replaced by a perch fixed to the side wall of the tunnel, which could be lowered by the experimenter. The training now changed focus. After the perch was lowered and the bird was flying, the perch was not raised until the bird flew in the desired position in the tunnel or displayed signs of fatigue. During this training phase the tunnel velocity was varied within the experimental range. When the bird was able to fly relatively stably in the desired location for 20–30 s the upstream net was removed and the experiments commenced.

Table 1. Individual characteristics

	Tailless	With tail
M (kg)	0.0163	0.0195
S_b (m^2)	0.00103	0.00115
U_{mp} (m s^{-1})	6.3	6.8
S (m^2)	0.0111	0.0105
b (m)	0.240	0.231
c (m)	0.046	0.046
AR	5.2	5.1

M, body mass; S_b, body frontal area; U_{mp}, minimum power speed; S, wing planform area; b, maximum wing span; c, mean chord length; AR, aspect ratio.

Experimental setup

The Lund University wind tunnel is a closed-loop, low-speed wind tunnel for studies of animal flight (Pennycuick et al., 1997). Background turbulence is about 0.04%, which makes this tunnel suitable for DPIV experiments (Spedding et al., 2008). All flight speeds (U) refer to the equivalent airspeed defined as:

$$U_{eq} = \sqrt{2q / \rho_0}\ , \quad (1)$$

where ρ_0 refers to the assumed air density at sea level in the International Standard Atmopshere (1.225 kg m^{-3}) and q ($=\rho U^2/2$) is the dynamic pressure at measured air density during an experiment. During this study the air density (ρ) varied between 1.16 and 1.19 kg m^{-3}, and the temperature was 21.1–26.3°C.

The birds were trained to fly in the centre of the test section and were studied at forward flight speeds of 6–10 m s^{-1} in 1 m s^{-1} intervals. The Reynolds number ($Re=Uc/\nu$, where U is airspeed, c is mean chord of the wing and ν is the kinematic viscosity) ranged between Re=17,500 and 29,500.

The flow velocity in three dimensions was measured in a plane of approximate size 20×20 cm^2 using two high-speed CMOS cameras (LaVision HighSpeedStar3; 1024×1024 pixels; Grove, Oxfordshire, UK) equipped with 60 mm lenses (Micro Nikkor, f2.8; Kingston upon Thames, UK), set up for stereo recording. The tunnel was filled with a thin fog (particle size ~1 μm), and the imaging plane was illuminated by a synchronized, pulsed, 50 mJ laser (Litron LPY732 series, Nd:YAG, 532 nm; Agawam, MA, USA) firing at 200 Hz repetition rate (f_{cam}). The light sheet was oriented transversely (in the [y, z] plane; Fig. 1) with the cameras mounted in the open part of the test section, viewing the light sheet obliquely from above and behind using Scheimpflug mounts to tilt the focal

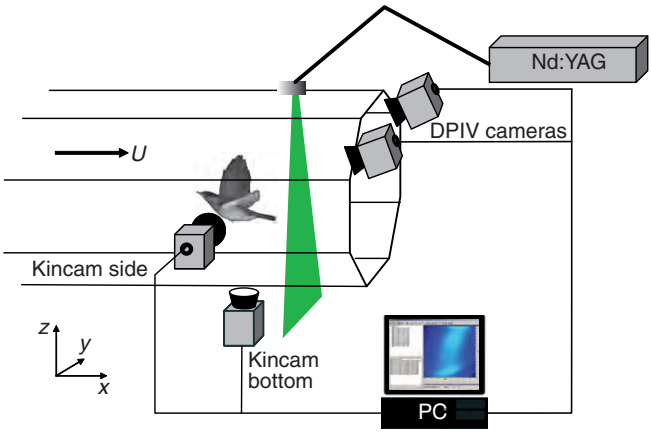

Fig. 1. Experimental setup. The bird is flying at speed U in the centre of the wind tunnel test section. The two kinematic cameras (Kincam) film the bird to determine the stability of the flight. The laser (Nd:YAG) generates a pulsed (200 Hz) light sheet perpendicular to the flow in the tunnel. Smoke particles in the light sheet are filmed by two synchronized high-speed DPIV cameras set up in stereo configuration to allow estimates of the out-of-plane velocity vector. The images are saved and analysed using commercial PIV-software (PC).

plane (Fig. 1). The DPIV cameras were equipped with band-pass filters (532±5 nm) to minimize stray light from other sources.

The DPIV data were captured and analysed using a commercial software package (LaVision, Davis 7.2.2.110; Grove, Oxfordshire, UK). The system was calibrated using a calibration plate ($20\times20\,cm^2$, type 22), in combination with a 'self-calibration routine', using captured images, to compensate for misalignments between the laser sheet and the calibration plate. During the experiments, but when the birds were not flying, regular measurements of the background flow were performed to determine accurate estimates of the flight speed.

In parallel with the DPIV measurements, two synchronized high-speed cameras (Redlake, MotionScope PCI 500, 250 Hz, 1/1250 s) recorded the birds from the side and from below. We used infrared illumination (VDI-IR60F, Video Security Inc., Kaohsiung, Taiwan) to minimize interference with the DPIV measurements, and the cameras were equipped with infrared filters [Schneider Optics, BW09249 092 (89B); Van Nuys, CA, USA] to eliminate the bright green flashes from the laser. The movies were used to visually determine the stability of the individual flights.

During experiments data were captured by manually triggering the system. When the bird was flying steadily in the centre of the tunnel the laser shutter was opened and the DPIV system triggered, capturing a sequence of 100 frames representing 0.5 s. The trigger signal simultaneously triggered the two high-speed cameras, capturing a video sequence (200 frames pre-trigger and 200 frames post-trigger) of the flying bird (Fig. 1).

Data analysis

The images were pre-processed by subtracting the sliding minimum (of five images), at each pixel, which reduces errors in the calculations due to background noise. The DPIV calculation settings were: a multi-pass stereo cross-correlation with decreasing correlation box size (first with 64×64 and then twice with 32×32, with 50% overlap). The last run was performed using the normalized correlation routine and Whittaker reconstruction. The analysis resulted in 5204 three-component vectors in each time step. The results were post-processed by deleting vectors if the peak ratio $Q<1.05$ and using a median filter removing vectors 1.5 r.m.s. above the average of the neighbouring vectors and inserting the second best vector if <2 r.m.s. above the average of the neighbouring vectors. Finally the data were smoothed once using a 3×3 box size (for the figures the data were smoothed a second time).

The algorithms used by Davis are the best commercially available (Stanislas et al., 2008). But to get an estimate of the accuracy of the DPIV analysis for this particular setup we determined the standard deviation of the out-of-plane velocity vectors within an image of the background flow. The standard deviation was relatively constant at ~1.5% across the used tunnel speed, which is in agreement with previous tests of the Davis algorithms (Stanislas et al., 2008). The error is well above the background turbulence in the tunnel and should be attributed to errors in the DPIV analysis (Spedding et al., 2009).

From a total of 447 sampled sequences, three sequences from each individual for each of the five speeds were chosen, based on stability of flight and position relative to the light sheet, for further analysis. In each sequence two or three wingbeats were analysed resulting in a total of 42 wingbeats for the tailless bird and 40 wingbeats for the bird with a tail. The resulting three-component velocity vector field of each time step was used to construct the vorticity field (ω_r) behind the bird using a custom-written Matlab program. The program was also used for measuring the vorticity and calculating the circulation (Γ) of vortices using the vorticity field. Because of the relatively large separation between frames (U/f_{cam}=0.05 m at a speed of 10 m s^{-1}) only the in-plane (streamwise) vorticity (ω_x) and circulation (Γ_x) could be calculated. The setup used here samples the wake at a more or less constant distance behind the bird as the wake moves through the light sheet. The wake is thus approximately of the same 'age' when it passes through the light sheet and the setup does not allow for the determination of wake evolution. The exact distance between the trailing edge of the wing and the light sheet differs slightly between different sequences (~9±4 x/c). However, previous studies of fixed wing wakes and the wakes of free-flying bats show that circulation is affected relatively little by the exact distance between the trailing edge within the range used here (Spedding et al., 2006; Johansson et al., 2008).

We determined the circulation of the wing tip and wing root vortices by selecting an area of interest, incorporating the wing tip or wing root area, and then integrated the vorticity above a cut-off value of ±70 s^{-1} over the area. The cut-off was set to be above 95% of the noise in the background, as determined from a set of background flows for the different speeds. Because absolute maximum vorticity during a wingbeat varied marginally over speed we chose to use a fixed cut-off value for all speeds. Assuming a normal distribution of the vorticity in the vortex we then added back the circulation below the cut-off value, following the procedures described in Spedding et al. (Spedding et al., 2003). A normal distribution of the vorticity in the vortices is supported by transects through the tip vortex (supplementary material Fig. S1) and previous studies of flying birds (Spedding et al., 1984). The circulation was normalized by dividing by Uc, as suggested by Spedding et al. (Spedding et al., 2003). We furthermore determined the peak positive and negative vorticity within the area of interest and the position of these maxima and minima was considered to be the centre of the vortices, which were subsequently used in the model for determining vertical and horizontal force. For the root area we calculated the mean circulation in each frame.

Force estimates

A simple vortex model was used to calculate the vertical force $\mathbf{F}_v$, or weight support (Rayner, 1979a; Rayner, 1979b; Rayner, 1979c; Spedding et al., 2003). We discretized the vortex model:

$$\mathbf{I}_z = \rho\Gamma S_e\,, \tag{2}$$

where $\mathbf{I}_z$ is the vertical impulse and S_e is the horizontally projected area of the wake, for each frame and summed the contributions over the wing beat [similar to Henningsson et al. (Henningsson et al., 2008)]. The vertical impulse for each frame was calculated as ρ multiplied by the circulation, in the plane of measurement, of the wing tip vortex of the left wing (Γ^-) (or dominant wing root vortex, a patch of vorticity positioned close to the wing root area, of the same sign), multiplied by the horizontally projected area. The area was estimated as twice the horizontal distance between the vortex centre and the centre of the body (b^-) multiplied by U and the time between frames ($1/f_{cam}$). From this the same estimate based on the dominant wing root vortex of opposite sign (Γ^+) was subtracted to generate the net vertical impulse for each time step. To generate the average vertical force the net impulse was summed over the wing beat and multiplied by the wing beat frequency (f), resulting in:

$$\mathbf{F}_v = \frac{\rho f U}{f_{cam}}\sum_1^n\left(\left|\Gamma_n^- b_n^-\right| - \left|\Gamma_n^+ b_n^+\right|\right), \tag{3}$$

where n is the number of frames during a wing beat and b^+ is twice the distance between the wing root vortex of opposite sign to the

wing tip vortex and the centre of the body. The model assumes that the circulation around the wing at each time step can be accurately described by the circulation of the streamwise vortices measured and that Eqn 2 can be applied at each time step. It also assumes that the circulation of the wing is constant along the span or that any deviation from this can be captured by the streamwise vortices (tip and root) found in the wake. Additionally, it assumes that the projected area of the wake can be approximated to a rectangle ($b_{\mathrm{wake}}U/f_{\mathrm{cam}}$) at each time step.

The estimated vertical force was compared with the weight of the animal and was used to estimate a vertical force coefficient according to:

$$C_{\mathrm{v}} = \frac{\mathbf{F}_{\mathrm{v}}}{qS}, \qquad (4)$$

where q (=0.5ρU^2) is the dynamic pressure and S is the wing planform area. This C_{v} is a mean coefficient assuming constant wing morphology and that the wings move through the air at the flight speed. It should not be confused with the lift coefficient (C_{l}) of the wing, which takes the wing's actual morphology and kinematics into account. For a more detailed analysis on how C_{l} can be estimated in flapping wings we refer to Dickson and Dickinson (Dickson and Dickinson, 2004).

Horizontal force ($\mathbf{F}_{\mathrm{h}}$) was estimated in a similar manner to the vertical force from the horizontal component of the impulse. The horizontal impulse was estimated as ρ multiplied by the circulation of the wing tip vortex (or wing root vortex of the same sign) multiplied by the projected area of the vortex structure on the transverse plane [y, z]. The projected area was considered to be the area swept by the wings in the transverse plane and was estimated as a triangle between the centre of the body, the centre of the vortex in the current frame and the mean point between the current position of the vortex and its position in the previous frame. To this the area of the triangle between the centre of the body, the centre of the vortex in the current frame and the mean point between the current position of the vortex and its position in the next frame was added (Fig. 2). This allowed us to take into account the fact that at the transitions between upstroke and downstroke and *vice versa*, the induced flow changes direction in the streamwise direction thus resulting in either positive or negative horizontal force. This model therefore differs from previous models (e.g. Spedding et al., 2003; Henningsson et al., 2008) in that the vortex is considered not to have rolled up to an elliptical structure but instead to retain the rather complex shape obtained when shed from the trailing edge. Any contribution of the wing root vortices to the horizontal force was considered small because of the small vertical movement of these vortices and their lower strength and was ignored in the calculations. The horizontal impulse was then summed over the wingbeat and multiplied by the wingbeat frequency to obtain the horizontal force. The horizontal force during a wingbeat was thus calculated according to:

$$\mathbf{F}_{\mathrm{h}} = \rho f \sum_{1}^{n} \Gamma_n^- \left(S_{\Delta(n-\frac{1}{2})} \left(\frac{z_n - z_{n-1}}{|z_n - z_{n-1}|} \right) + S_{\Delta(n+\frac{1}{2})} \left(\frac{z_{n+1} - z_n}{|z_{n+1} - z_n|} \right) \right), \qquad (5)$$

where S_{Δ} is the area of the triangle and the subscripts n–½ and n+½ refer to the triangle based on the vortex position in the current and in the preceding frame, and the current and proceeding frame, respectively. z is the vertical position of the centre of the vortex and the inner expressions involving z determine whether the normal of the triangle is tilting backwards or forwards in the flight direction (i.e. whether the vortex contributes to positive or negative horizontal force). Using the vertical and horizontal force estimates we calculated a ratio $\mathbf{F}_{\mathrm{v}}/\mathbf{F}_{\mathrm{h}}$. The horizontal force was also used to estimate a horizontal force coefficient according to:

$$C_{\mathrm{h}} = \frac{\mathbf{F}_{\mathrm{h}}}{qS}. \qquad (6)$$

The C_{h} estimated here is subject to the same assumptions as discussed above regarding the C_{v}.

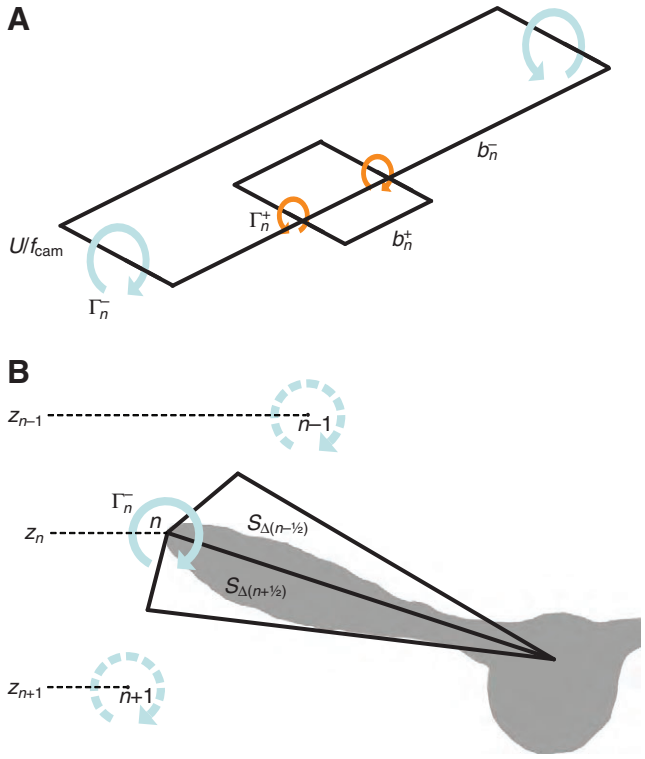

Fig. 2. Geometric model for calculating the impulse in each frame. (A) Vertical force calculations. The image illustrates the horizontally projected area of the wake between the wing tip vortices and wing root vortices as seen from above and behind at an early stage of the downstroke. Γ^- is the circulation of the wing tip or wing root vortex. Γ^+ is the circulation of the wing root vortex (during early stages of the downstroke). b^- is the wake width of the tip or root vortices, and b^+ is the wake width of the wing root vortices during the early stages of the downstroke. U/f_{cam} is the distance the air moves between frames due to the wind tunnel speed. (B) Horizontal force calculations. The image shows the rear view [y, z] of the left wing and the bird prior to mid-downstroke. Γ^- is the circulation of the wing tip or wing root vortex. S_{Δ} is the area of the triangle and the subscripts n–½ and n+½ refer to the triangle based on the vortex position in the current and in the preceding frame and the current and proceeding frame, respectively. z is the vertical position of the centre of the vortex. The sum of the two triangles represents the area swept by the wing between frames.

Statistics

To allow for comparisons within wing beats between individuals and speeds we fitted a spline function to each wing beat and estimated the values for the variables of interest for the average number of frames during a wing beat in the entire dataset (which was 12 frames). The mean value and standard error for each time step (T_{norm}) during the wing beat for each individual and speed were then determined using an ANOVA with sequence as a random factor.

We tested for differences between the bird with and the bird without a tail using a mixed linear model. The model was set up

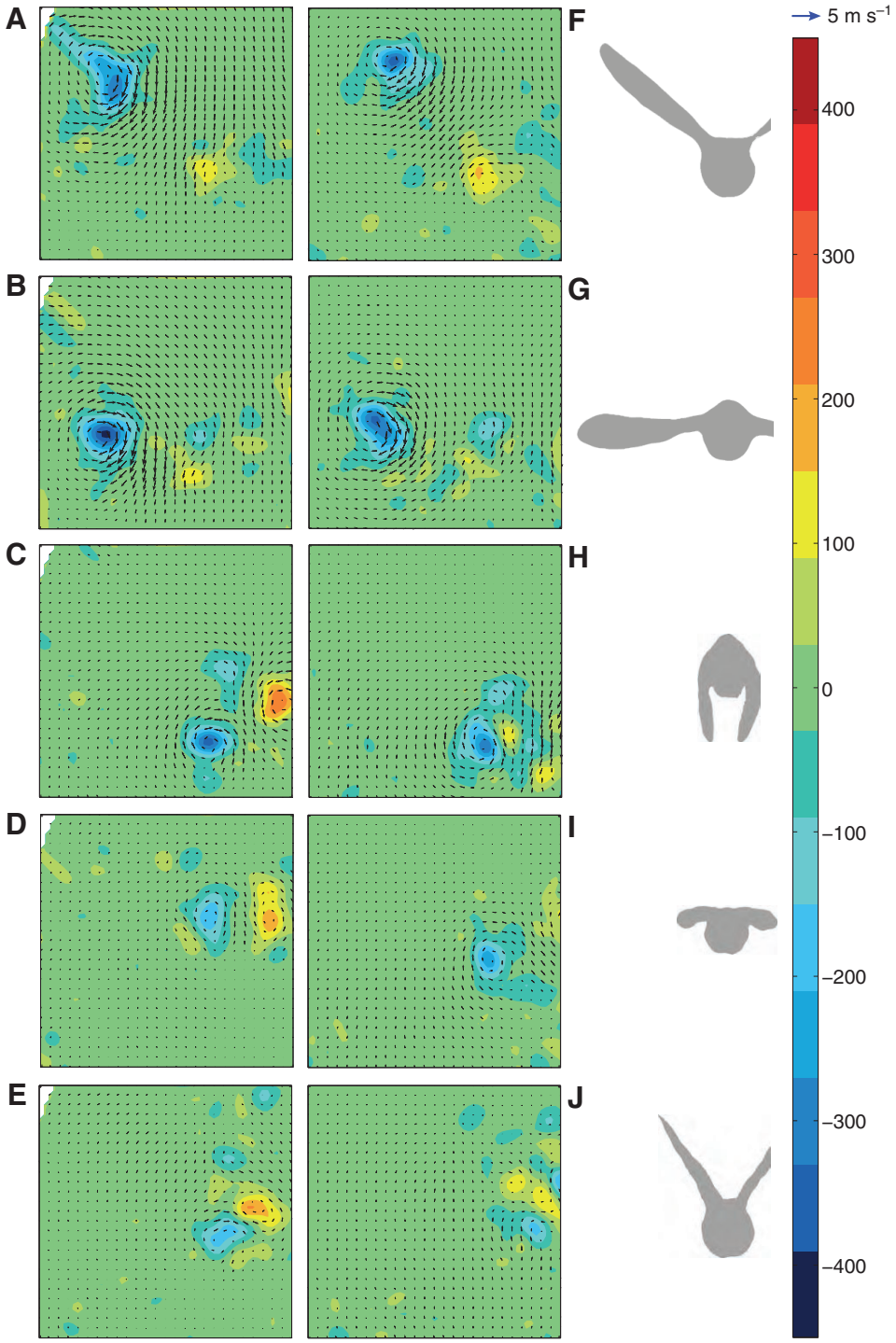

Fig. 3. Velocity and vorticity fields (ω_x) from the transverse plane [*y*, *z*] behind a bird with a tail (A–E) and a bird without a tail (F–J) flying at 8 m s^{-1}. The vorticity/velocity fields are from the beginning of the downstroke (A,F), mid-downstroke (B,G), end of the downstroke (C,H), mid-upstroke (D,I) and end of the upstroke (E,J). The vorticity is colour coded according to the colour bar on the right and the vectors are scaled according to the reference vector above the colour bar.

with the natural logarithm of the mean normalized circulation of the wing tip vortex ($\bar{\Gamma}_{tip}/Uc$) for each sequence, or normalized mean wing root circulation ($\bar{\Gamma}_{root}/Uc$), C_v, C_h or $\mathbf{F}_v/\mathbf{F}_h$ as dependent variables. We normalized the flight speed by dividing by the calculated minimum power speed, U_{mp}, as suggested by Rosén et al. (Rosén et al., 2007). The minimum power speed was estimated according to Pennycuick's Flight v. 1.17 model (Pennycuick, 1989):

$$U_{mp} = \left(\frac{W}{\rho}\right)^{1/2} \left(\frac{4k_i}{3S_b C_d \pi b^2}\right)^{1/4}, \quad (7)$$

where W is the weight, k_i (=1.2) is the induced power factor, S_b is the frontal area of the body, C_d is the body drag coefficient and b is the wing span. S_b was estimated using the empirically established formula S_b=0.00813×$m^{0.666}$ (Pennycuick, 1989). With or without tail was set as a fixed factor and the natural logarithm of U/U_{mp} was used as a covariate. We included the interaction between the factor and the covariate in the model. The analysis was performed using JMP® 8.0 (SAS Institute Inc.). Use of the natural logarithm to linearize the data was motivated by the fact that Γ/Uc is expected to be proportional to U^{-2} (Johansson et al., 2009).

RESULTS

Vortex wake morphology

When the downstroke begins, a strong start vortex is shed from the trailing edge of the wing. Although spanwise vorticity is not measurable in the transverse plane, the out-of-plane velocity shows decreased speed above and increased speed below a line connecting the wing tip vortex and the centre of body plane, indicative of an oblique cut through a start vortex. Also, one frame before the wing tip vortex is visible in the image, an upwash is visible where the wing is expected to be, indicative of a cut just outside a start vortex (Fig. 3E,J). During the build up of the circulation of the wing tip vortex in the first part of the downstroke, a streamwise vortex of the opposite sense of rotation is visible close to the wing root (Fig. 3A,F). When reaching mid-downstroke, or slightly after, weak or no vorticity is visible in the wing root area (Fig. 3B,G). As the stroke progresses further a vortex of the same sense as the wing tip vortex becomes visible near the wing root area. At the end of the downstroke the wing tip vortex becomes weaker again (Fig. 3C,H) and as the wing is folded during the upstroke, the wing tip vortex merges with the wing root vortex (Fig. 3D,I). The wing root vortex of the same sense as the wing tip vortex remains present throughout the upstroke (Fig. 3E,J) and does not disappear until the wing root vortex of the opposite sense is visible (Fig. 3A,F). There are no visible differences in the wake pattern between the bird with (Fig. 3A–E) and the bird without a tail (Fig. 3F–J).

In order to generate a model of the wake based on the transverse data, we made isosurface plots (using the Matlab function isosurface) of the vorticity in the wake (Fig. 4) (for the tailless bird see supplementary material Fig. S2). The plots summarize the description above and suggest that the wake is best described as closed vortex loops generated during the downstroke with a rather inactive upstroke. During the upstroke the body/tail and the partly folded wings generate a vortex structure contributing to vertical force generation, but with a small relative horizontally projected area.

We also plotted isosurfaces of the out-of-plane velocity field, relative to the flight speed (u_r–U) (Fig. 5) (for the tailless bird see supplementary material Fig. S3). Although these are helpful when constructing the wake model, they should be interpreted with caution. As discussed above, out-of-plane velocity is not necessarily the result of negative or positive horizontal force generation, but can also be the consequence of cutting obliquely through a vortex. The out-of-plane velocity isosurface plot shows high positive and negative relative velocities at the beginning of the downstroke. This is the cut through the start vortex, and the figure shows that the start vortex is almost perpendicular to the flight direction. As the stroke progresses we see a decreased velocity near the wing tip, which partly is due to the ‘upwash’ outside the wing tip vortex, which is tilted forwards because of the flapping of the wing. At the end of the downstroke, the wing tip vortex and the associated decreased velocities move towards the body and during the upstroke we mainly see what we interpret as body drag. Air flow with increased speed relative to the flight speed can be found between the wing tip vortices, mainly during the downstroke. As for the decreased speed, some of this increased speed is due to cutting obliquely through the wing tip vortex and some of it represents the horizontal force generated. It is worth noting that increased speed can also be found across the body, despite the body drag reducing the speed, connecting the flow between the two wings during part of the downstroke. At the end of the downstroke and beginning of the upstroke the flow of each wing is seemingly separated by the body. A potential reason is that the vortex structure follows the trailing edge of the wing, and because the wing tips are below the body, at this phase of the wing beat, it results in an inverted V- or U-shape of the wake. It is likely that some of the decreased and increased velocities we see at the end of the downstroke/beginning of the upstroke are due to cutting through a stop vortex. The stop vortex is then directed more obliquely relative to the flight direction than the start vortex.

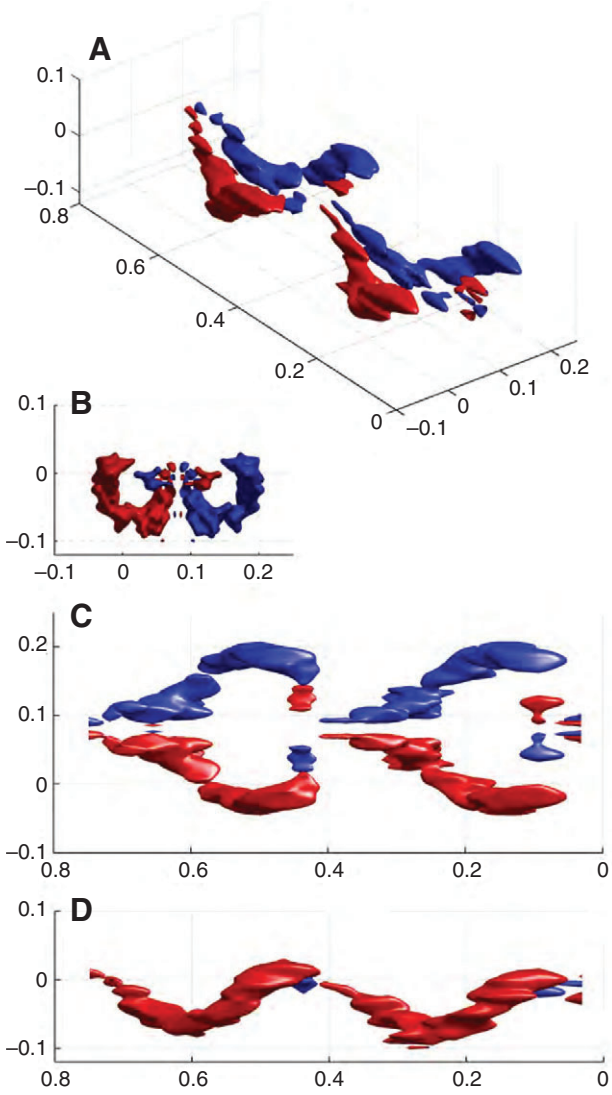

Fig. 4. Isosurface plots of the streamwise vorticity (WT vort, ω_x) in the wake of the bird with a tail at 6 m s^{-1} flight speed, viewed obliquely from above (A), from behind [y, z] (B), straight from above [Ut, y] (C) and from the side [Ut, z] (D). The vorticity field did not include the entire span of the bird, so the data were mirrored at the centre plane of the body (determined as the centre between the left and right wing root vortices) to facilitate interpretation of the wake. No blending or smoothing was done and the mirroring did not visibly affect the wake topology. Iso values were set at –90 s^{-1} (red) and +90 s^{-1} (blue).

Isosurface plots of the vertical induced velocities show similar patterns to the out-of-plane velocity (Fig. 6) (for the tailless bird see supplementary material Fig. S4). At the beginning of the downstroke we see an upwash followed by a downwash, which is the cut through the start vortex. Throughout the rest of the downstroke we then see an upwash caused by the wing tip vortex surrounding an area of downwash between the wing tip vortices. Some of the downwash

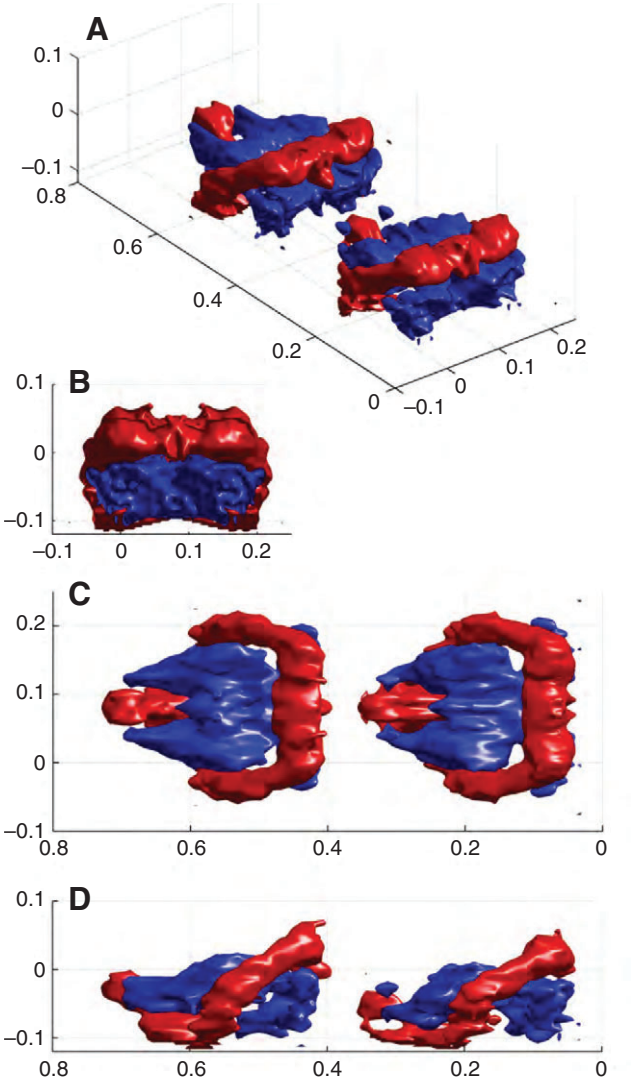

Fig. 5. Isosurface plots of the out-of-plane velocity relative to the flight speed in the wake of the bird with a tail at 6 m s^{-1} flight speed viewed obliquely from above (A), from behind [*y*, *z*] (B), straight from above [*Ut*, *y*] (C) and from the side [*Ut*, *z*] (D). The velocity field did not include the entire span of the bird, so the data were mirrored at the centre plane of the body (determined as the centre between the left and right wing root vortices) to facilitate interpretation of the wake. No blending or smoothing was done and the mirroring did not visibly affect the wake topology. Iso values were set at *U*–0.5 m s^{-1} (red) and *U*+0.5 m s^{-1} (blue).

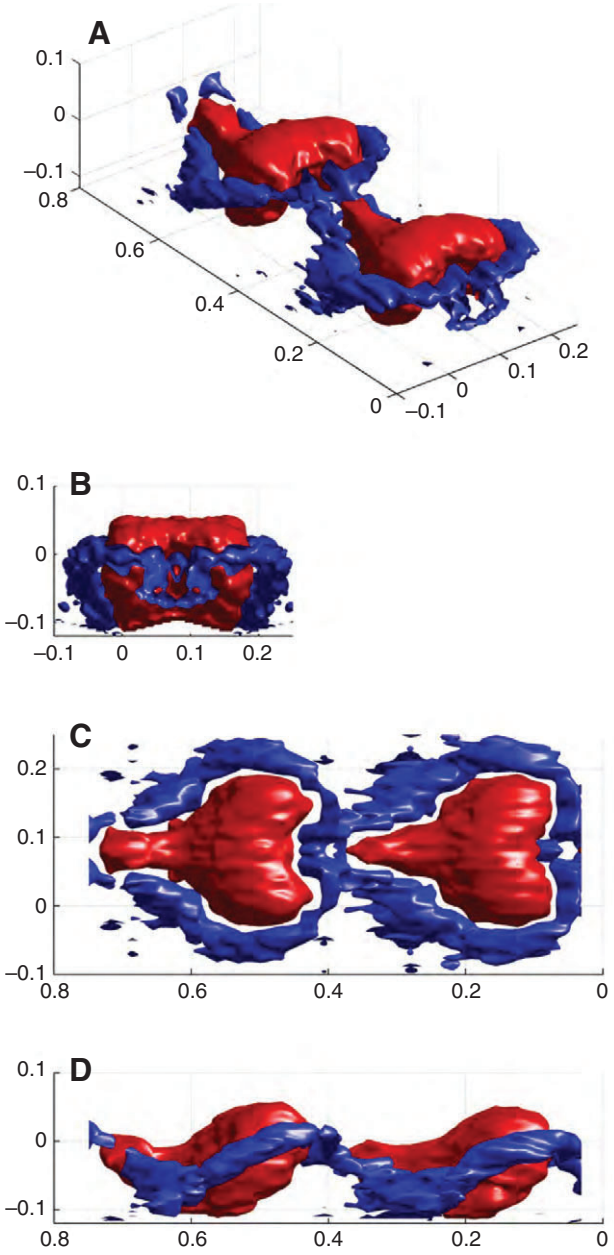

Fig. 6. Isosurface plots of the vertical velocity in the wake of the bird with a tail at 6 m s^{-1} flight speed viewed obliquely from above (A), from behind [*y*, *z*] (B), straight from above [*Ut*, *y*] (C) and from the side [*Ut*, *z*] (D). The velocity field did not include the entire span of the bird, so the data were mirrored at the centre plane of the body (determined as the centre between the left and right wing root vortices) to facilitate interpretation of the wake. No blending or smoothing was done and the mirroring did not visibly affect the wake topology. Iso values were set at –0.65 m s^{-1} (red) and +0.65 m s^{-1} (blue).

seen is due to the wing tip vortex. Until mid-upstroke, the body, tail and partly folded wings generate some downwash.

Quantitative wake data

The normalized circulation of the wing tip vortex increases steeply during the downstroke until about 40% of the stroke duration and then decreases more slowly to zero by the end of the upstroke (Fig. 7). As expected, the mean absolute normalized circulation of the wing tip vortex decreases with increasing flight speed (Fig. 8A). There was no significant difference between the bird with and the bird without a tail (P=0.36, d.f.=1, power=0.15).

The normalized wing root circulation shows a pattern of circulation of opposite sense to the wing tip vortex during the beginning of the downstroke followed by zero net circulation during mid-downstroke. At the end of the downstroke and throughout the upstroke the net wing root circulation has the same sign as the wing tip vortex with maximum values during mid-upstroke (Fig. 7). As for the wing tip vortex the net normalized wing root circulation, summed over the wing beat, decreases with increasing flight speed and has on average the same sign as the wing tip vortex (Fig. 8B). There was no significant difference between the bird with and the bird without a tail (P=0.64, d.f.=1, power=0.075).

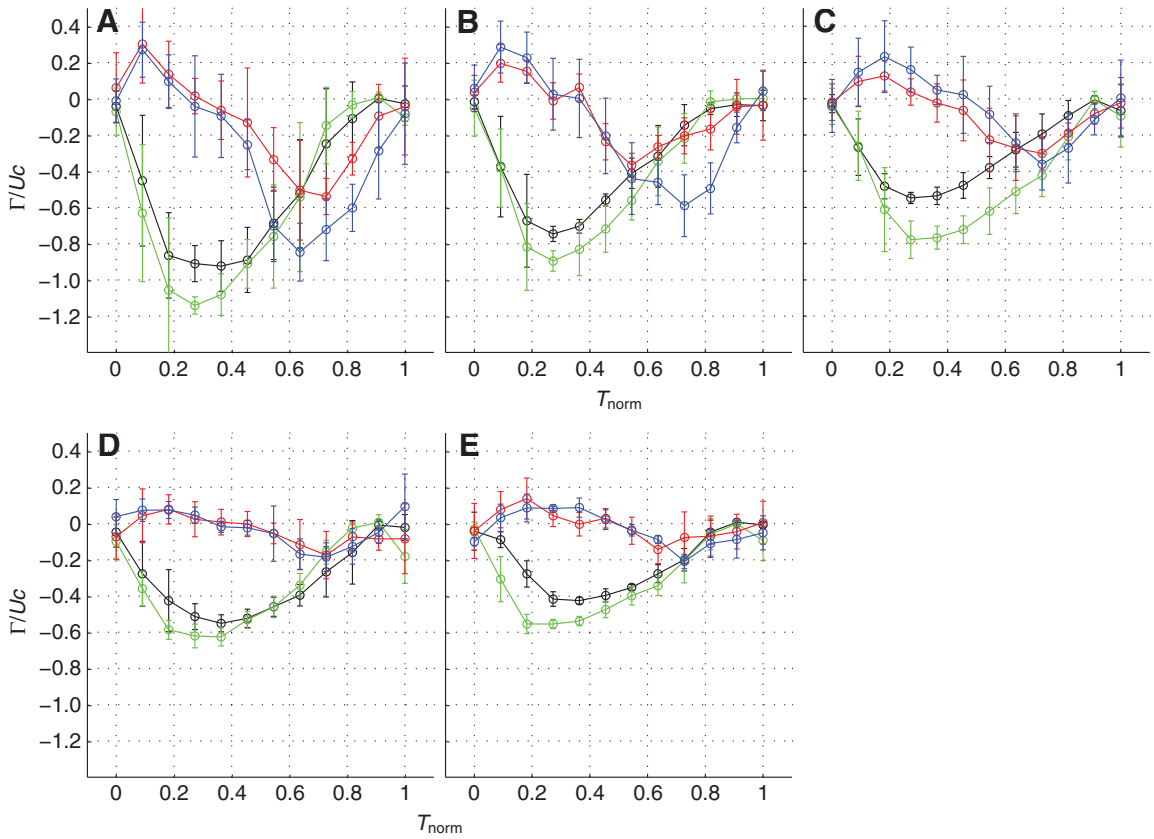

Fig. 7. Normalized circulation (Γ/Uc) of the wing tip vortex and wing root area during normalized wing beats (T_{norm}), at flight speeds of 6 m s^{-1} (A), 7 m s^{-1} (B), 8 m s^{-1} (C), 9 m s^{-1} (D) and 10 m s^{-1} (E). The values are means ± s.e.m. Bird with tail: tip, green; root, blue. Bird without tail: tip, black; root, red.

The vertical impulse follows a similar pattern to the wing tip vortex circulation, with a steep increase at the beginning of the downstroke, reaching a maximum at mid-downstroke, and then decreasing throughout the remainder of the downstroke and the upstroke (Fig. 9). Zero vertical impulse is found at the transition of the upstroke/downstroke at low flight speeds, while at higher flight speeds there may be a small but continuous production of positive vertical impulse (Fig. 9). The net vertical force generated by the vertical impulse agrees well with the weight of the animals. The mean vertical force of the tailless bird is 99.7±4.7% (mean±s.e.m.) of the weight, and for the bird with a tail it is 105.2±3.1%. The vertical force coefficient based on the wing planform area varies between 0.16 and 1.3, with decreasing values with increasing flight speed (Fig. 10). There was no difference between the birds with and without a tail (P=0.194, d.f.=1, power=0.25).

The horizontal impulse shows a similar, but also distinctly different, pattern to the vertical impulse. The increase in force production at the beginning of the downstroke is more modest and the decrease after the peak is more pronounced (Fig. 11). Also, at all speeds there is negative horizontal force generated during parts of the upstroke (Fig. 11). The horizontal force coefficient based on the wing planform area varies between 0.051 and 0.21, with

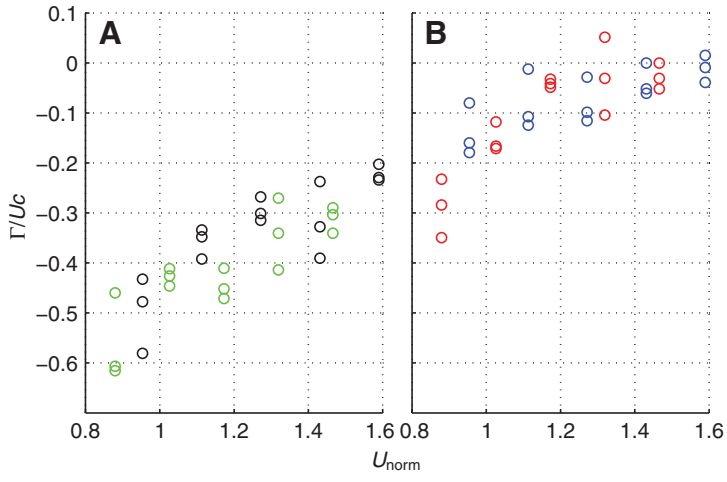

Fig. 8. Mean normalized circulation (Γ/Uc) of the wing tip vortex (A) and wing root area (B) for each measured sequence plotted against flight speed normalized with minimum power speed ($U_{norm}=U/U_{mp}$). Bird with tail: tip, green; root, blue. Bird without tail: tip, black; root, red.

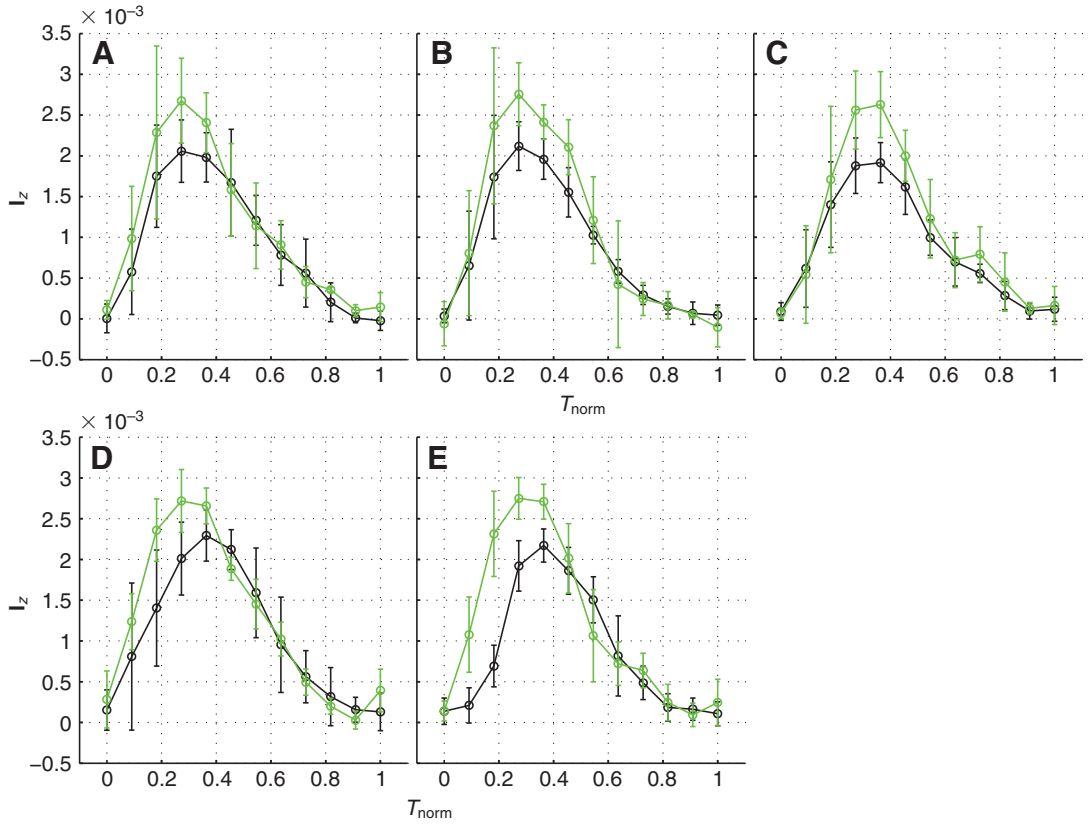

Fig. 9. Net vertical impulse ($\mathbf{I}_z$) during normalized wing beats (T_{norm}), at flight speeds of 6 m s^{-1} (A), 7 m s^{-1} (B), 8 m s^{-1} (C), 9 m s^{-1} (D) and 10 m s^{-1} (E). Positive values indicate force generation adding to weight support. The values are means ± s.e.m. Bird with tail: green. Bird without tail: black.

decreasing values with increasing flight speed (Fig. 12). There was a significant difference between the bird with and the bird without a tail (P=0.0036, d.f.=1), with the bird with a tail showing higher values.

The estimated $\mathbf{F}_v/\mathbf{F}_h$ varied between 2.7 and 7.6, and values decreased with increasing speed (Fig. 13). There was a significant difference between the bird with and the bird without a tail (P=0.0092, d.f.=1), with the bird without a tail having the higher values.

DISCUSSION

Vortex wake morphology

Previous wake studies of birds have constructed models of the wake based on streamwise [x, z] measurements at different positions along the span. This is excellent for measuring spanwise variation in circulation and also for determining temporal variation in circulation throughout the wing beat. However, estimating streamwise vorticity is not possible and recent studies of bat wakes have pointed to the importance of streamwise data for the reconstruction of the wake topology (Hedenström et al., 2007; Johansson et al., 2008). In previous work, the wakes of birds have been modelled as a gradual shift between two extremes, with a closed vortex loop model at low speeds and a continuously changing circulation model at high speeds (Spedding et al., 2003; Henningsson et al., 2008). In the models suggested so far, the wake structures of the individual wings are connected over the body, generating a unified vortex structure for the two wings. In the current study we found some support for this view (Figs 5 and 6), but conclude that the picture is a bit more complicated. Our results support a downstroke-dominated positive vertical and horizontal force generation, with some positive vertical force generation also during the upstroke (Figs 9 and 11) and gradual changes in the circulation around the wings (Fig. 7). In this sense, the wake pattern of the blackcap is similar to the wake suggested for high flight speed for the thrush nightingale (Spedding et al., 2003). However, we also found wing root vortices not previously described in birds. The presence of wing root vortices of opposite

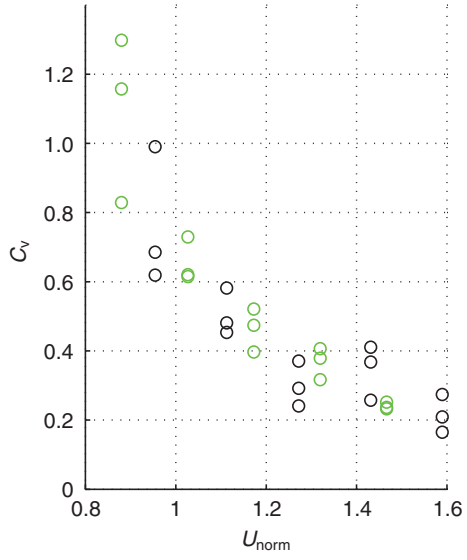

Fig. 10. Mean vertical force coefficient (C_v) for each sequence estimated from the vertical force and the wing planform area, plotted against flight speed normalized with minimum power speed (U_{norm}=U/U_{mp}). Bird with tail: green. Bird without tail: black.

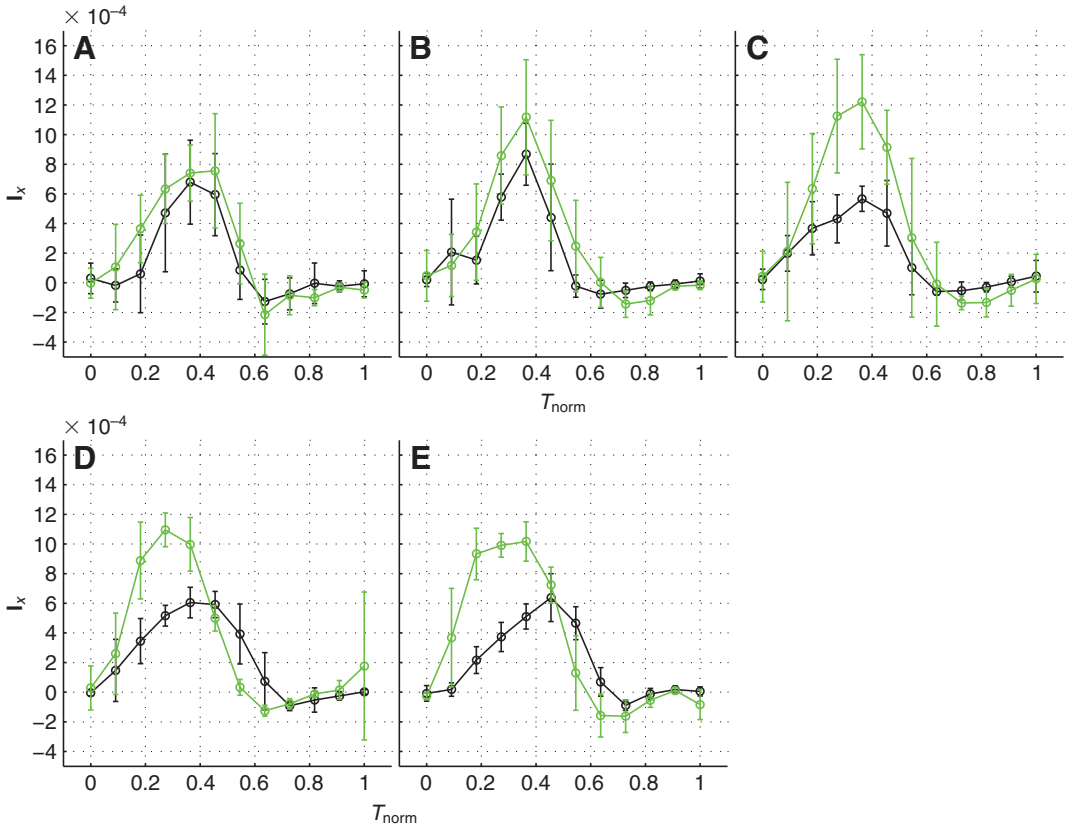

Fig. 11. Net horizontal impulse ($\mathbf{I}_x$) during normalized wing beats (T_{norm}), at flight speeds of 6 m s^{-1} (A), 7 m s^{-1} (B), 8 m s^{-1} (C), 9 m s^{-1} (D) and 10 m s^{-1} (E). Positive impulse indicates thrust and negative impulse indicates negative thrust. The values are means ± s.e.m. Bird with tail: green. Bird without tail: black.

sense to the wing tip vortex during the first half of the downstroke is similar to what has been found in bats (Hedenström et al., 2007; Johansson et al., 2008; Hedenström et al., 2009). However, the wing root vortices of the same sense as the wing tip vortices found during the second half of the downstroke have previously not been described, either in birds or in bats. The wing root vortices are indicative of gradients in the circulation along the span between the wing and the body (Rossow, 1973). Also, wing root vortices of opposite sense to the wing tip vortices during the initial part of the downstroke suggest a lower circulation at the body than at the wings. In contrast, wing root vortices of the same sense as the wing tip vortices during the second part of the downstroke would suggest a higher circulation at the body/tail than at the wings. This indicates that the wings function at least partially independently during the downstroke or, to put it differently, that the body does not have the same circulation as the wings throughout the downstroke.

Table 2. Mean wing beat frequency (f) and reduced frequency (k=fc/U) across flight speeds

	f (Hz)		k	
	Tailless	With tail	Tailless	With tail
6 m s^{-1}	17.1	17.5	0.13	0.13
7 m s^{-1}	16.8	18.6	0.11	0.12
8 m s^{-1}	16.7	19.1	0.096	0.11
9 m s^{-1}	17.9	18.4	0.092	0.094
10 m s^{-1}	17.7	18.7	0.081	0.086

Force generation

We have used relatively simple models to estimate the forces generated from the measured circulation and wake morphology. Despite this simplicity, the estimated vertical force during a wing

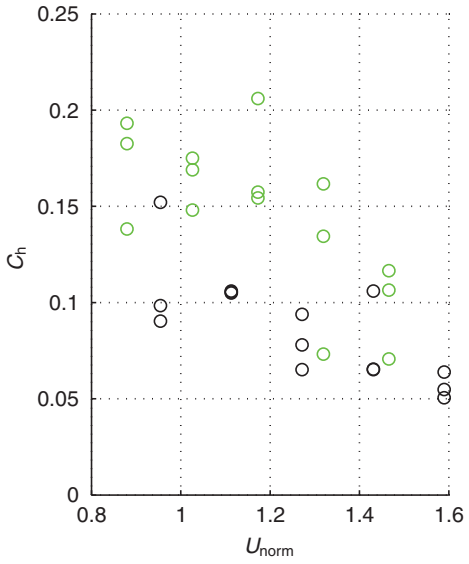

Fig. 12. Mean horizontal force coefficient (C_h) for each sequence estimated from horizontal force and the wing planform area, plotted against flight speed normalized with minimum power speed (U_{norm}=U/U_{mp}). Bird with tail: green. Bird without tail: black.

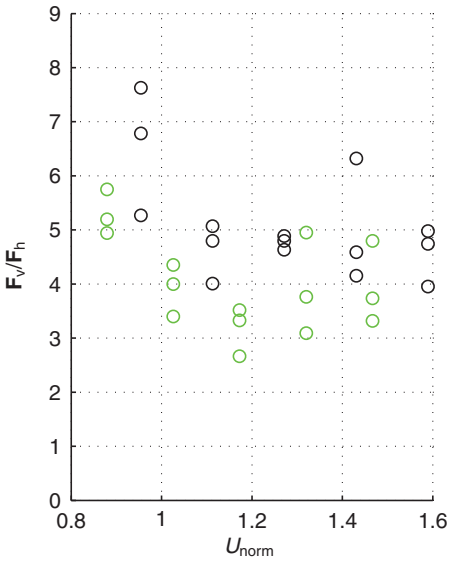

Fig. 13. Vertical to horizontal force ratio, $\mathbf{F}_v/\mathbf{F}_h$, plotted against flight speed normalized with minimum power speed ($U_{norm}=U/U_{mp}$). Bird with tail: green. Bird without tail: black.

beat agrees well with the weight of the birds, which increases our confidence in the estimated horizontal force. The horizontal force coefficients estimated here are, however, relatively high (Fig. 12). Comparing the horizontal force coefficient estimated for swifts at a Re=2.2×10^4 (Henningsson et al., 2008) with the horizontal force coefficient estimated here at a similar Re shows that the horizontal force of the blackcaps is 50–130% higher than for the swifts. The rather high horizontal force is also reflected in the low $\mathbf{F}_v/\mathbf{F}_h$ values (Fig. 13), compared with the swifts [$\mathbf{F}_v/\mathbf{F}_h$=13.3 for swifts (Henningsson et al., 2008)]. This could reflect differences in body drag coefficients, with the swifts being more streamlined than the blackcaps, or differences in the induced drag, with swift wings generating less drag than blackcap wings. It could, however, also reflect differences in flight style. The swifts studied were juveniles flying for the first time in their life in the tunnel (Henningsson et al., 2008). Although this could suggest suboptimal flight performance, the birds do not have any experience of flying in the wild and thus there is nothing to suggest that flying in the tunnel is out of the ordinary in any way. The blackcaps on the other hand were adults caught in the wild. When flying initially in the tunnel, they displayed strong signs of manoeuvring flight (extremely stationary flight, hanging feet, premature exhaustion), but as we trained them these signs disappeared. Although we have made an effort to select data from sequences when the birds do not show any signs of manoeuvring, it might be that the birds still perform some sort of subtle manoeuvring flight. This could include flying with the body and/or wings at suboptimal angles of attack, which would increase the required horizontal force and thus increase the horizontal force coefficient. Using birds trained from juveniles as well as testing multiple species will be required to resolve this matter.

Function of the tail

We did not find support for the hypothesis that the tail should function as a splitter plate to reduce the drag of the birds (Maybury and Rayner, 2001). In fact, the estimated horizontal force coefficient (which corresponds to the overall drag coefficient) is higher for the bird with the tail (Fig. 12), suggesting a higher drag with the tail. However, the effect of the tail of an actively flying bird, might be relatively small compared with the effect on a mounted bird without wings as used by Maybury and Rayner (Maybury and Rayner, 2001). Considering our low sample size the results should be interpreted with some caution and to properly test this hypothesis we would prefer to perform more detailed measurements with and without the tail on the same individual. This would remove any uncertainties caused by differences in, for example, flight style between the two individuals. It would also allow direct measurement of the decreases in the out-of-plane dynamic pressure in the body area (which is related to the body drag) when the tail is removed. However, Tobalske and colleagues (Tobalske et al., 2009) found an increase in the body drag coefficient when increasing the tail length from zero to 150% of the original length, in zebra finches mounted as during bounding flight, which is thus consistent with our results for flapping flight.

We found no support for the hypothesis that the tail should reduce the cost of flight by utilizing the induced flow between wing root vortices. From this hypothesis it would, for example, be predicted that wing root vortices, of the opposite sense of rotation to the wing tip vortices, should be present in the tailless bird throughout the downstroke [as is the case in bats (Hedenström et al., 2007; Johansson et al., 2008; Hedenström et al., 2009)]. In the bird with the tail these wing root vortices would, optimally, either be absent or have reduced circulation. Not only did we find no differences in the wake morphology between the two birds but also none of the normalized quantitative measures of circulation differed. Furthermore, the wake pattern found did not match any of the two expected wake morphologies outlined above. Also, in a thrush nightingale, where we studied the wake of the same individual, with and without a tail (using a 10 Hz, two-dimensional DPIV setup), we found no qualitative or quantitative differences in the wake (L.C.J., personal observation). We thus conclude that this hypothesis is not supported by the data, at least in these two species. During steady level flight the tail is often furled in birds, which is a potential explanation for why we find no differences between the bird with and the bird without a tail. During manoeuvres the tail is spread, which will result in the tail being better positioned to utilize the wing root vortices, and the tail presumably has a more aerodynamically active function than during steady flight.

Concluding remarks

Here we have presented the first results of DPIV measurements in the transverse plane behind a free-flying bird during forward flight. We found novel wake structures previously not shown in birds, including wing root vortices of opposite as well as the same sign as the wing tip vortices. This suggests a more complex wake structure in birds than previously assumed and calls for more detailed studies of the flows over the wings and body. We were unable to detect any effects on the wake pattern caused by the tail during steady flight in blackcaps with and without a tail. We thus conclude that the birds do not use the tail to exploit vortices shed at the wing root during the downstroke, at least not during steady level flight. The difference in strength of the wing tip and wing root vortices suggests above-zero circulation at the body, and isosurface plots of the induced downwash also suggest some lift production at the body. Lift generated by the body during at least the upstoke has been observed for zebra finches based on DPIV measurements (Tobalske et al., 2009), which supports our findings that the body plays a role in weight support during active flight in blackcaps.

LIST OF ABBREVIATIONS

b	wing span
b^-	wake width of the tip or root vortices
b^+	wake width of the wing root vortices
c	mean wing chord
C_d	body drag coefficient
C_h	horizontal force coefficient
C_l	wing lift coefficient
C_v	vertical force coefficient
f	wing beat frequency
f_cam	frame rate of the camera
$\mathbf{F}_\mathrm{h}$	horizontal force
$\mathbf{F}_\mathrm{v}$	vertical force
$\mathbf{I}_x$	horizontal impulse
$\mathbf{I}_z$	vertical impulse
k_i	induced power factor
n	number of frames during a wing beat
q	dynamic pressure
S	wing planform area
S_b	frontal area of body
S_e	horizontally projected area of wake
S_Δ	area of triangle
t	time
T_norm	duration of normalized wing beat
U	flight speed
U_mp	mimimum power speed
W	weight
z	vertical position of the centre of the vortex
Γ	vortex circulation
Γ_root	circulation of wing root vortex
Γ_tip	circulation of wing tip vortex
ν	kinematic viscosity
ρ	air density
ρ_0	assumed air density at sea level
ω_r	vorticity field
ω_x	streamwise vorticity

We are grateful to F. T. Muijres and P. Henningsson for comments on the horizontal force model and to R. von Busse for assisting during experiments. This work was supported by grants from the Swedish Research Council, the Knut and Alice Wallenberg Foundation, the Crafoord Foundation, the Magnus Bergvall Foundation, and the Royal Physiographical Society in Lund. A.H. is a Swedish Royal Academy of Sciences Research Fellow supported by a grant from the Knut and Alice Wallenberg Foundation.

REFERENCES

Brown, R. H. J. (1953). The flight of birds. II. Wing function in relation to flight speed. *J. Exp. Biol.* **30**, 90-103.

Dickson, W. B. and Dickinson, M. H. (2004). The effect of advance ratio on the aerodynamics of revolving wings. *J. Exp. Biol.* **207**, 4269-4281.

Hedenström, A., Rosén, M. and Spedding, G. R. (2006a). Vortex wakes generated by robins *Erithacus rubecula* during free flight in a wind tunnel. *J. R. Soc. Interface* **3**, 263-276.

Hedenström, A., van Griethuijsen, L., Rosén, M. and Spedding, G. R. (2006b). Vortex wakes of birds: recent developments using digital particle image velocimetry a wind tunnel. *Anim. Biol.* **56**, 535-549.

Hedenström, A., Johansson, L. C., Wolf, M., von Busse, R., Winter, Y. and Spedding, G. R. (2007). Bat flight generates complex aerodynamic tracks. *Science* **316**, 894-897.

Hedenström, A., Muijres, F., von Busse, R., Johansson, L. C., Winter, Y. and Spedding, G. R. (2009). High-speed stereo DPIV measurement of wakes of two bat species flying freely in a wind tunnel. *Exp. Fluids* **46**, 923-932.

Hedrick, T. L., Tobalske, B. W. and Biewener, A. A. (2002). Estimates of circulation and gait change based on a three-dimensional kinematic analysis of flight in cockatiels (*Nymphicus hollandicus*) and ringed turtle-doves (*Streptopelia risoria*). *J. Exp. Biol.* **205**, 1389-1409.

Hedrick, T. L., Usherwood, J. R. and Biewener, A. A. (2004). Wing inertia and whole-body acceleration: an analysis of instantaneous aerodynamic force production in cockatiels (*Nymphicus hollandicus*) flying across a range of speeds. *J. Exp. Biol.* **207**, 1689-1702.

Henningsson, P., Spedding, G. R. and Hedenström, A. (2008). Vortex wake and flight kinematics of a swift in cruising flight in a wind tunnel. *J. Exp. Biol.* **211**, 717-730.

Johansson, L. C., Wolf, M., von Busse, R., Winter, Y., Spedding, G. R. and Hedenström, A. (2008). The near and far wake of Pallas' long tongued bat (*Glossophaga soricina*). *J. Exp. Biol.* **211**, 2909-2918.

Johansson, L. C., Wolf, M. and Hedenström, A. (2009). A quantitative comparison of bird and bat wakes. *J. R. Soc. Interface* doi:10.1098/rsif.2008.0541.

Maybury, W. J. and Rayner, J. M. V. (2001). The avian tail reduces body parasite drag by controlling flow separation and vortex shedding. *Proc. Biol. Sci.* **268**, 1405-1410.

Norberg, U. M. (1975). Hovering flight in the pied flycatcher (*Ficedula hypoleuca*). In *Swimming and Flying in Nature*, vol. 2 (ed. T. Y. T. Wu, C. J. Brokaw and C. Brennen), pp. 869-881. New York: Plenum Press.

Norberg, U. M. (1990). *Vertebrate Flight*. Berlin: Springer Verlag.

Pennycuick, C. J. (1989). *Bird Flight Performance: A Practical Calculation Manual.* Oxford: Oxford University Press.

Pennycuick, C. J., Alerstam, T. and Hedenström, A. (1997). A new low-turbulence wind tunnel for bird flight experiments at Lund University, Sweden. *J. Exp. Biol.* **200**, 1441-1449.

Rayner, J. M. V. (1979a). A vortex theory of animal flight. I. The vortex wake of a hovering animal. *J. Fluid Mech.* **91**, 697-730.

Rayner, J. M. V. (1979b). A vortex theory of animal flight. II. The forward flight of birds. *J. Fluid Mech.* **91**, 731-763.

Rayner, J. M. V. (1979c). A new approach to animal flight mechanics. *J. Exp. Biol.* **80**, 17-54.

Rosén, M., Spedding, G. R. and Hedenström, A. (2007). Wake structure and wingbeat kinematics of a house-martin *Delichon urbica*. *J. R. Soc. Interface* **4**, 659-668.

Rossow, V. J. (1973). On the inviscid rolled-up structure of lift-generated vortices. *J. Aircraft* **10**, 647-650.

Spedding, G. R., Rayner, J. M. V. and Pennycuick, C. J. (1984). Momentum and energy in the wake of a Pigeon (*Columba livia*) in slow flight. *J. Exp. Biol.* **111**, 81-102.

Spedding, G. R., Rosén, M. and Hedenström, A. (2003). A family of vortex wakes generated by a thrush nightingale in free flight in a wind tunnel over its entire natural range of flight speeds. *J. Exp. Biol.* **206**, 2313-2344.

Spedding, G. R., McArthur, J. and Rosén, M. (2006). Deducing aerodynamic mechanisms from near- and farwake measurements of fixed and flapping wings at moderate Reynolds number. AIAA 2006-33, 44th AIAA Aerospace Sciences Meeting and Exhibit, Reno, Nevada.

Spedding, G. R., Hedenström, A. H., McArthur, J. and Rosen, M. (2008). The implications of low-speed fixed-wing aerofoil measurements on the analysis and performance of flapping bird wings. *J. Exp. Biol.* **211**, 215-223.

Spedding, G. R., Hedenström, A. and Johansson, L. C. (2009). A note on wind-tunnel turbulence measurements with DPIV. *Exp. Fluids* **46**, 527-537.

Stanislas, M., Okamoto, K., Kähler, C. J., Westerweel, J. and Scarano, F. (2008). Main results of the third international PIV Challenge. *Exp. Fluids*, **45**, 27-71.

Thomas, A. L. R. (1993). On the aerodynamics of birds' tails. *Philos. Trans. R. Soc. Lond. B Biol. Sci.* **340**, 361-380.

Thomas, A. L. R. (1997). On the tails of birds. *Bioscience* **47**, 215-225.

Tobalske, B. W., Hearn, J. W. D. and Warrick, D. R. (2009). Aerodynamics of intermittent bounds in flying birds. *Exp. Fluids*. **46**, 963-973.

Warrick, D. R., Tobalske, B. W. and Powers, D. R. (2005). Aerodynamics of the hovering hummingbird. *Nature* **435**, 1094-1097.

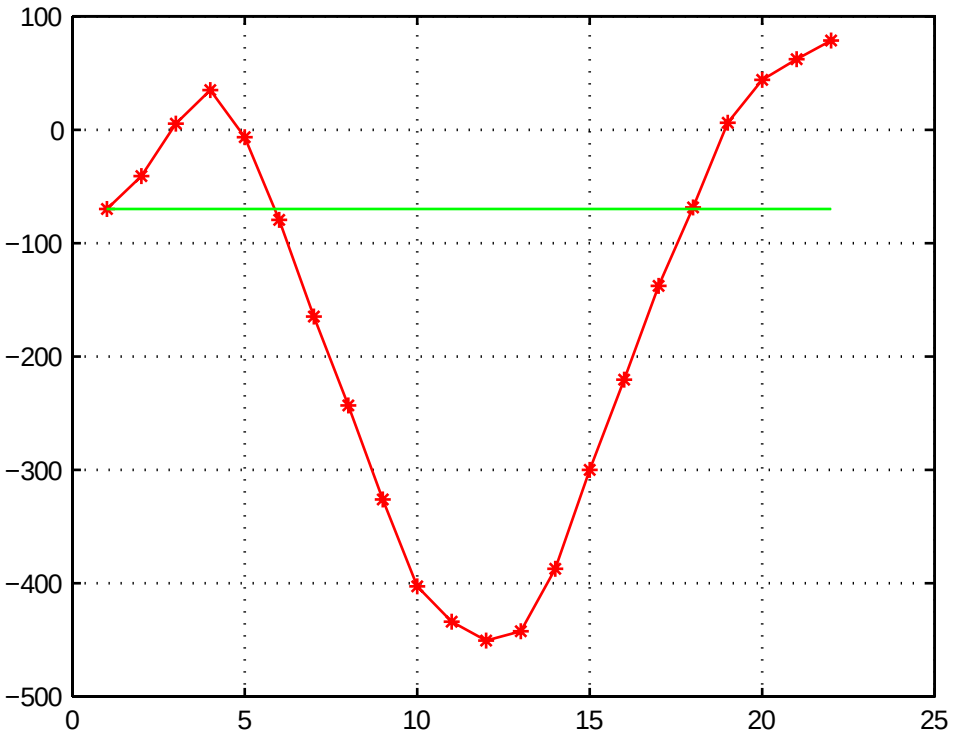
100
0
−100
−200
−300
−400
−500
0
5
10
15
20
25

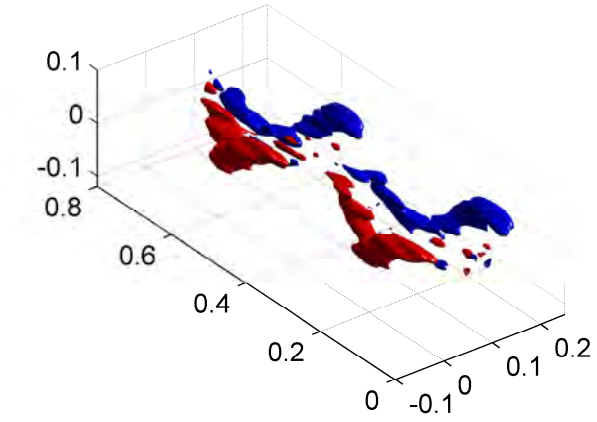
0.1
0
-0.1
0.8
0.6
0.4
0.2
0
-0.1
0
0.1
0.2

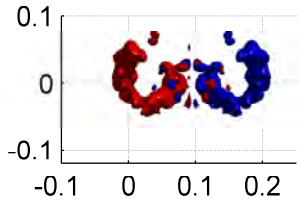
0.1
0
-0.1
-0.1
0
0.1
0.2

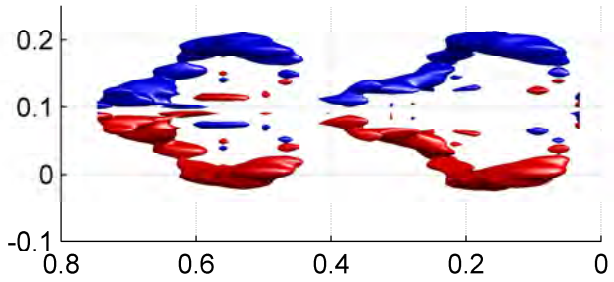
0.2
0.1
0
-0.1
0.8
0.6
0.4
0.2
0

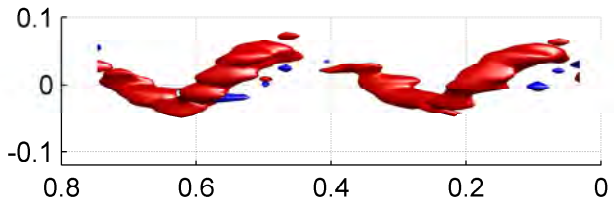
0.1
0
-0.1
0.8
0.6
0.4
0.2
0

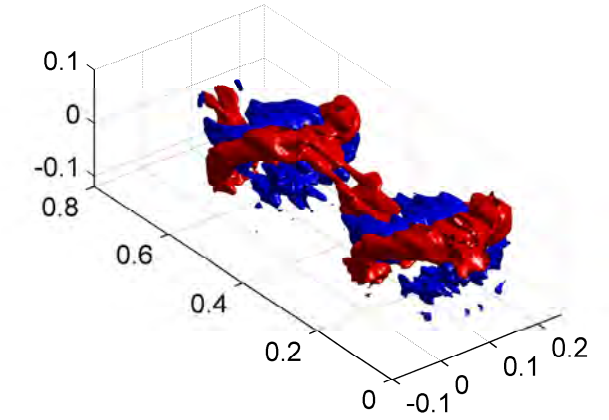
0.1
0
-0.1
0.8
0.6
0.4
0.2
0
-0.1
0
0.1
0.2

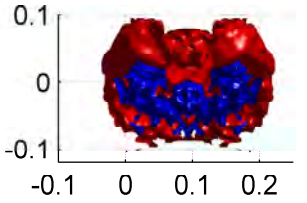
0.1
0
-0.1
-0.1
0
0.1
0.2

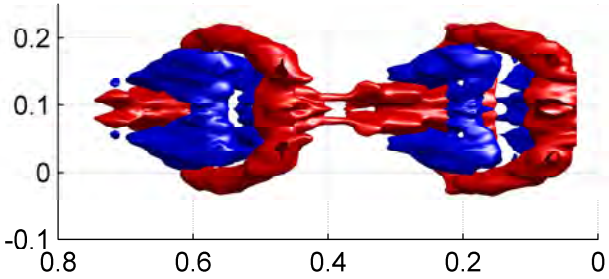
0.2
0.1
0
-0.1
0.8
0.6
0.4
0.2
0

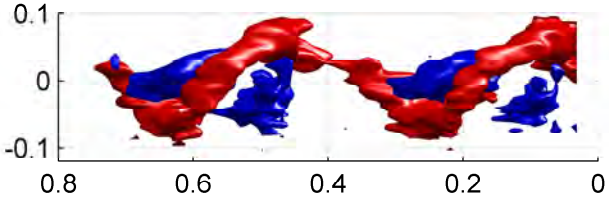
0.1
0
-0.1
0.8
0.6
0.4
0.2
0

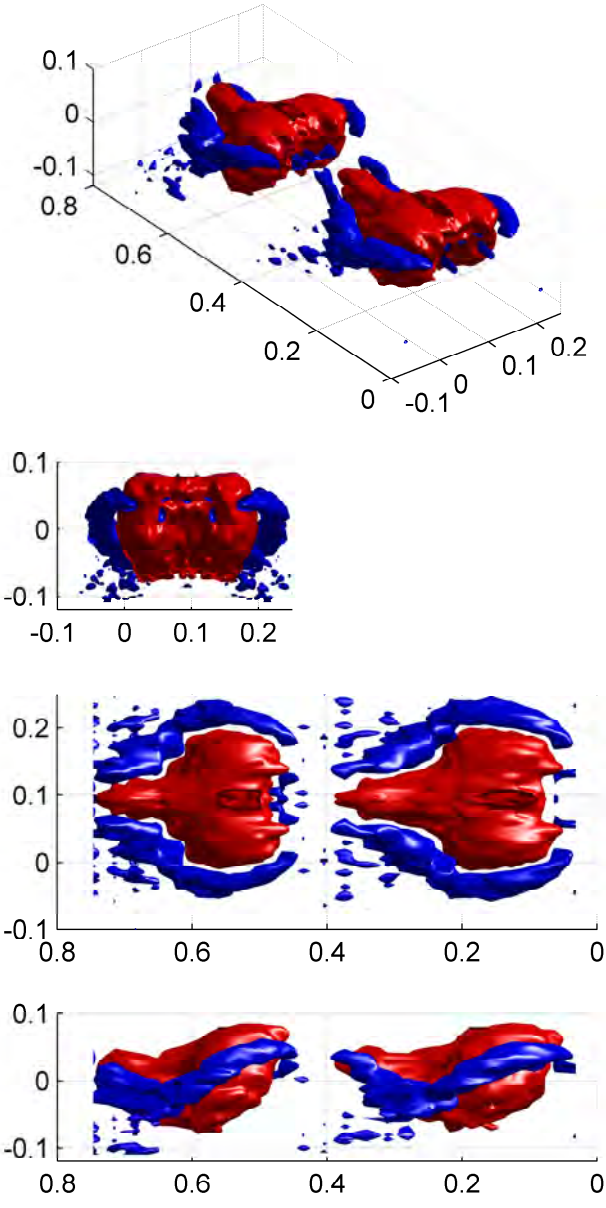
0.1
0
-0.1
0.8
0.6
0.4
0.2
0
-0.1
0
0.1
0.2
0.1
0
-0.1
-0.1
0
0.1
0.2
0.2
0.1
0
-0.1
0.8
0.6
0.4
0.2
0
0.1
0
-0.1
0.8
0.6
0.4
0.2
0